Journal of Materials Chemistry A

Accepted Manuscript

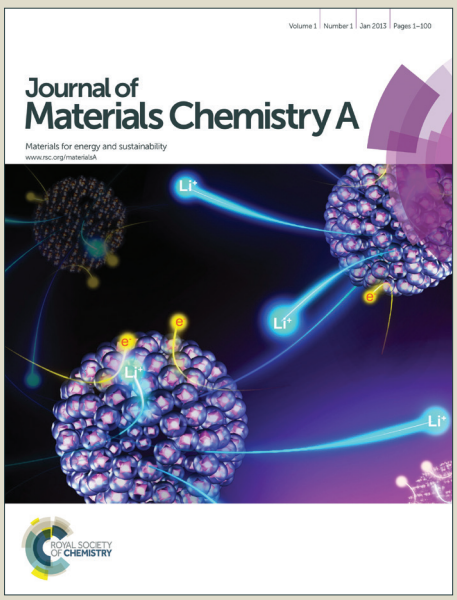

ROYAL SOCIETY OF CHEMISTRY

www.rsc.org/materialsA

Self-assembly of graphene oxide aerogels by layered double hydroxides cross-linking and their application in water purification

Qile Fang; Baoliang Chen*

(Department of Environmental Science, Zhejiang University, Hangzhou, Zhejiang 310058, China; Zhejiang Provincial Key Laboratory of Organic Pollution Process and Control, Hangzhou 310058, China)

* Corresponding Author E-mail: blchen@zju.edu.cn

Phone: 0086-571-88982587

Fax: 0086-571-88982587

Table of Contents

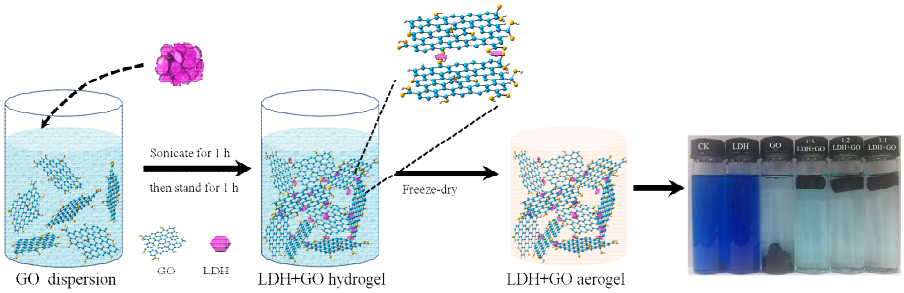

3D macrostructural aerogels were synthesized based on the self-assembly of graphene oxide and LDHs, which exhibited excellent hydrophilicity, structural stability, and superior adsorption properties in water purification.

Abstract

Self-assembly based on graphene building blocks are an important strategy for three-dimensional (3D) architectures, but their fabrication and application in water purification remain challenging. Here, we report a facile one-step approach to prepare 3D graphene oxide (GO) hydrogels and aerogels containing nanoscaled layered double hydroxides (LDHs). The LDHs acted as cross-linking agent molecules ("buttons") to join GO nanosheets into a 3D network via charge-assisted hydrogen bonds and lattice-lattice cation-π interactions. The resultant aerogels exhibited high hydrophilicity, excellent structural stability/plasticity in water environments, which guarantee the availability of their effective active sites in aqueous solution and overcome the utilization restrictions of neat GO aerogels due to their fragile morphology. The obtained LDH+GO aerogels showed super capability for removal of dye (methylene blue) and heavy metal (Cd^{2+}) pollutants from water. The addition of LDHs nanoparticles assisted the aerogels in well maintaining their 3D monoliths and made it easy for separation and collection after use, and improved the adsorption capacities for environmental pollutants via reducing the stacking of GO sheets and exposing more active adsorption sites. Thus the obtained LDH+GO aerogels have a great potential for water purification as high-efficient and stable adsorbents.

1. Introduction

Self-assembling nanostructures into three-dimensional (3D) hierarchical architectures has been recognized as one of the most promising strategies for "bottom-up" nanotechnology,[1] as it is of special relevance for macroscopic applications and the development of nanomaterials.[2,3] Graphene, the first available two-dimensional (2D) atomic carbon crystal, has quickly emerged as a "rising star" on the horizon of materials science.[4,5] 3D self-assembly of graphene and its functionalized derivatives has fascinated scientists for the last two or three years, primarily in respect that the high-performance graphene-based superstructures not only take advantage of the initial and novel collective physiochemical properties of graphene, but also the 3D network prevents aggregation and guarantees mass transport, consequently enhancing performance.[3,6-11] However, great challenges remain in the design and synthesis of these new materials of macrostructures (organogels, hydrogels, and aerogels) due to the lack of knowledge of the sol-gel chemistry of graphene.

To circumvent the poor dispersibility of pristine graphene, graphene oxide (GO) has been alternatively employed as a building block for superstructure assembly because it is rich in oxygen-containing groups, resulting in excellent dispersibility in most polar solvents.[3,12] Graphene superstructures can then be obtained via chemical and thermal reduction of the 3D GO network precursor.[13-15] Moreover, the abundant functional groups on the GO edges/surfaces not only give rise to the high chemical reactivity of GO gels but also offer ample modification potential due to the simple fabrication process.[16-18] Meanwhile, the main disadvantage of GO hydrogels or aerogels is their extreme fragility, such that the resultant structures fail to maintain a well-defined 3D morphology, limiting their utility.[19,20] Therefore, different cross-linking agent molecules have been evaluated to improve the mechanical stability of GO superstructures through physical and chemical cross-linking, including polymers,[18,21-23] small organic molecules,[19,24] biomacromolecules (DNA or protein),[25,26] and multivalent ions (La^{3+}, Fe^{2+}, Ni^{2+}, Ca^{2+} and Co^{2+}).[18,27,28] Recent studies of metal [29,30]

and metal oxides nanoparticles [31-34] formed *in situ* and uniformly distributed in GO architectures have evoked broad interest in a new type of 3D architecture based on organic-inorganic nanomaterials. But the formations of these complex GO monoliths were all impelled by extra hydrothermal treatment or other additives as cross-linking/reducing agents.

The synthesized 3D graphene macrostructures have preliminarily exhibited their great potential in the fields of energy,[35-37] catalysis,[38] sensors,[39] biotechnology,[40,41] and environment.[23,24,42-45] Especially in the control of environmental pollutants, although graphene behaved excellent removal capacities,[45] environmental risk of material itself and hard for regulation are the two main problems in the application of the nanomaterial. Self-assembled 3D graphene macrostructures can felicitously solve this issue and simultaneously maintain the superior performance of graphene in water purification.

Here, we report a unique route to fabricate 3D GO hydrogels and aerogels via the self-assembly of 2D GO sheets cross-linked by layered double hydroxides (LDHs), another large class of multifunctional materials whose inorganic nanolamellar and positively charged frameworks make it wide use in various fields.[46] Different from previous reports of the integration of metal (metal oxide) nanoparticles into GO hydrogels, a facile one-step approach was successfully employed for LDH+GO hydrogel formation in the present study without any hydrothermal processing or additives. With a proper ratio of organic and inorganic components, Mg-Al LDHs acted as cross-linking agent molecules, well prevented their layered crystal structure and uniformly cross-linked GO sheet into a 3D network structure through strong/weak hydrogen bonds, electrostatic interactions, and cation-π interactions. As a result of these multiple interactions, the assembled GO aerogels exhibited high hydrophilic properties and excellent structural stability in aqueous solution, which simultaneously improved the accessibility of active sites on graphene in aqueous solution. The obtained LDH+GO aerogels showed powerful capability for removal of dye and heavy metal pollutants from water, and the well maintained 3D monoliths made it easy for separation and collection.

2. Experimental

2.1 Materials. Natural graphite powder (325 mesh) was obtained from Alfa Aesar. All the chemicals were analytical purity without further purification and purchased from Sinopharm Chemical Reagents Co. Ltd. (China). GO was prepared from natural graphite powders based on the Hummers method with some modification.[47] Mg-Al-CO_3^{2-} LDHs were synthesized by a conventional co-precipitation method with an Mg/Al ratio of 4.[48] The detailed processes are illustrated in the ESI.

2.2 Preparation of LDH-assembled GO hydrogels and aerogels. Synthesis of LDH-assembled GO hydrogels (LDH+GO hydrogels) was carried out in two sets. In the first set, the addition of LDH powder was fixed at 5 mg mL^{-1}, and the concentration of the homogeneous GO dispersion was varied from 5 to 1 mg mL^{-1}, resulting in five samples with LDH:GO ratios of 1:1, 2:1, 3:1, 4:1, and 5:1. In the second set, the concentration of the GO dispersion was fixed at 5 mg mL^{-1}, and the concentration of LDH was varied from 1 to 5 mg mL^{-1} to produce five samples with LDH:GO ratios of 1:5, 1:4, 1:3, 1:2, and 1:1. The different samples and their LDH:GO ratios are listed in Table S-1 (ESI). After adding the LDHs to the GO dispersion, the heterogeneous mixture was shaken and then sonicated for 1 h. The mixture was then allowed to stand at room temperature for 1 h to permit the formation of LDH+GO hydrogels. Finally, the 3D dark-brown monoliths were further freeze-dried into LDH+GO aerogels.

2.3 Characterization. The microstructures and elemental distribution of the aerogels were characterized using an FE-SEM equipped with an EDS (SU-70, Hitachi), HR-TEM/SAED at an acceleration voltage of 200 kV, and STEM (Tecnai G2 F20 S-TWIN, FEI). FT-IR was recorded in the region of 4000-400 cm^{-1} with a Thermo Nicolet FT-IR spectrophotometer (model 6700) with a resolution of 1.0 cm^{-1}. Raman experiments were performed on a LabRAM HR UV spectrometer (Horiba Jobin Yvon) with excitation by a 514.5 nm line from an Ar^+ laser and a resolution of 1.0 cm^{-1}. XRD profiles were obtained using a Rigaku D/max-2550PC diffractometer with Cu Kα radiation (λ = 0.15406 nm). The thermal

stability of the samples was measured by TGA using a TG analyzer (Tagongsi SDTQ600, USA) under a nitrogen atmosphere, with heating from room temperature to 700 ˚C at a rate of 5 ˚C min^{-1}.

2.4 Adsorption experiments. Methylene blue (MB), one type of cationic dyes, was chosen as the model dyes compounds to test the removal capacities of assembled LDH+GO aerogels. Adsorption experiments were carried out at an initial MB concentration of 20 mg L^{-1}, and four aerogel monoliths with different LDH:GO ratios were added. After shaken for 48h at 25 ± 1 ˚C, the apparent equilibrium concentration of MB solutions was measured using an UV/Vis spectrometer and calculated by the absorbance at 664 nm.[49] The control tests with only LDHs powder (solid-to-solution ratio of 5 mg/40 mL) and without any adsorbents were also conducted. Cd^{2+} was selected as a representative of heavy metal pollutants. Time-dependent adsorptions using the assembled aerogel monoliths were carried out at initial Cd^{2+} concentration of 50 mg L^{-1}. At predetermined time intervals, concentrations of the metal ions were analyzed with a Perkin-Elmer Analyst 700 (PE700, USA) atomic absorption spectrometer. Similarly, tests of blank and LDHs powder alone were also set. Meanwhile, the solution pH was monitored. The removal rate (%) and specific adsorbed amount (q) of pollutant (MB and Cd^{2+}) was calculated according to the following equation:

$$\text{Removal rate (\%)} = 100\% \times \boldsymbol{(C_o - C_t)/C_o}$$

$$q = (C_o - C_t) \times V/m$$

where C_o and C_t are the initial and specific time (t) concentrations of pollutants (mg L^{-1}); V is the volume of aqueous solution (mL); and m is the mass of the aerogels and LDH powder (mg).

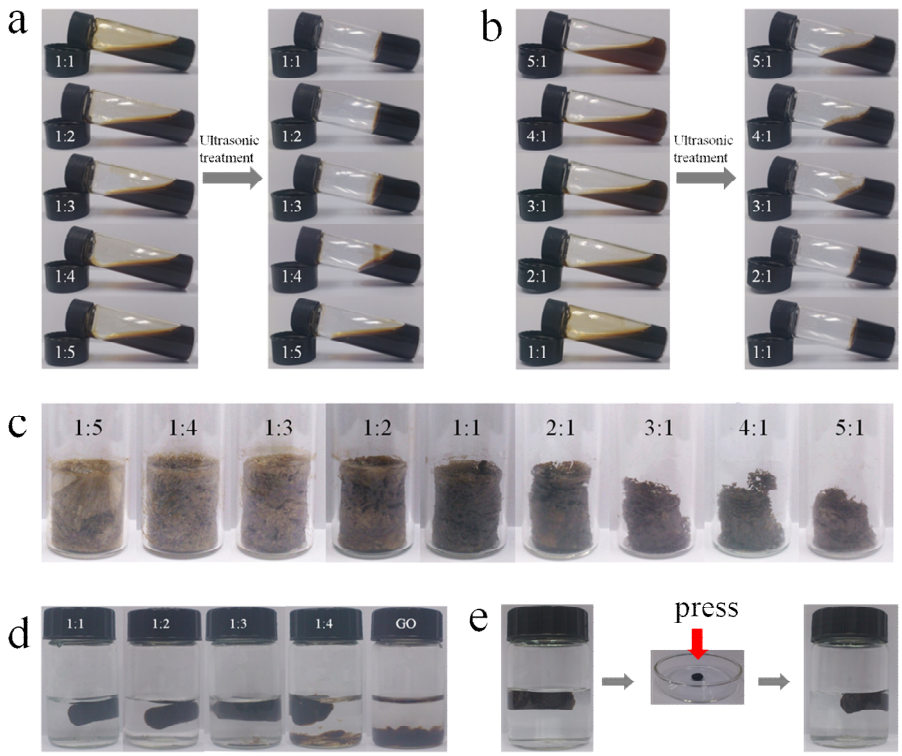

Fig. 1 Images of the formation process for LDH+GO hydrogels and aerogels. (a) Hydrogel formation after ultrasonic treatment of the mixture of the aqueous GO dispersion (5 mg mL^{-1}) and different concentrations of LDH (5 mg mL^{-1}→1 mg mL^{-1} for 1:1→1:5 samples). (b) Mixtures of the LDH powder (5 mg mL^{-1}) and different concentrations of the aqueous GO dispersion (1 mg mL^{-1}→5 mg mL^{-1} for 5:1→1:1 samples). (c) Aerogel formation after freeze-drying of the sonicated mixtures. (d) Aerogel stability in aqueous solutions with mechanical vibration. (e) Water swelling and shape recovery of the pressed 1:1 aerogel in an aqueous solution.

3. Results and discussion

The facile synthesis of 3D LDH+GO monoliths, as shown in Fig. 1(a, b), was initiated under ultrasonic-assisted treatment of the mixture of GO suspension and LDH powder. As shown in the images acquired before and after ultrasonic assistance (Fig. 1a, b), hydrogel formation is sensitively dependent on the concentration of GO and LDHs. When the GO dispersion concentration was fixed at 5 mg mL^{-1} (Fig. 1a), the GO sheets crosslinked into a stable hydrogel only at an LDH:GO ratio ≥

1:3. Notably, the volume shrinkage was almost negligible for the resultant hydrogels, in contrast to some GO hydrogels prepared by other methods.[13,28,50] However, when the ratio of LDH to GO was less than 1:4, no monolith gelation was observed, but the dispersion seemed to be more viscous, or no visible change occurred. After sonication for 1 h, the original brown mixture became darker, indicating that the assembly of GO might involve interactions between GO and the LDHs. Similarly, when the amount of LDH powder was fixed at 5 mg mL^{-1}, the GO dispersion concentration also dramatically affected hydrogel fabrication (Fig. 1b). A stable hydrogel was formed only when the concentration of GO was ≥ 2.5 mg mL^{-1}, that is, only samples with ratios of LDH:GO of 2:1 and 1:1 formed stable solid gels. The remaining 3 mixtures became more viscous but did not gelate completely. Thus, the GO dispersion concentration and the LDH concentration are the two determining factors for gel formation; below specific threshold concentrations of each of these components, the two-dimensional GO cannot assemble into a 3D structure.

The hydrogels were subsequently freeze-dried to remove structural solvent (H_2O) and to fabricate the aerogels. As shown in Fig. 1c, increasing the LDH:GO ratio from 1:5 to 5:1 changed the color of the aerogels from dark yellow to dark brown. Changing the ratio of LDH:GO from 2:1 to 5:1, samples appear fluey and shrunken shapes and fall apart when touched. These results indicate that a GO concentration of less than 2.5 mg mL^{-1} is insufficient to support GO assembly into an entirely stable 3D network after lyophilization. Although no gelation occurred for the low LDH samples, such as the 1:5 LDH+GO sample, columned aerogels were formed, similar to the formation of spongy aerogels by neat GO upon freeze-drying.[14,43] Thus, low LDH:GO-ratio aerogels possessed a yellow color and foam texture similar to that of GO aerogels.

GO can assemble into hydrogels or aerogels via different cross-linking interactions, which are principally based on the hydrophilic properties and homogeneous dispersion of GO.[19] However, these properties also limit their applications as to that GO aerogels fall apart and disperse once they

are exposed to aqueous solution, like the neat GO aerogel shown in Fig. 1d. Thus, studies have focused on the synthesis of graphene aerogels by the reduction of GO gels, which present a hydrophobic surface[51] and exhibit superior performance for oil or organic solvent sorption.[44] However, the self-assembled GO aerogels crosslinked by LDHs in this study possessed both high hydrophilic properties and aqueous environment stability. As shown in Fig. 1d, LDH+GO aerogels with ratios of 1:1 to 1:3 remained intact upon immersion in an aqueous solution, even under physical shaking, while 1:4 LDH+GO aerogels and neat GO aerogels displayed weak structural stabilities.

High plasticity is another key advantage of LDH-crosslinked GO aerogels. As shown in Fig. 1e, water-saturated LDH+GO aerogels could be pressed into a circular flake, thus removing most of the water. Thereafter, the flattened layer was immersed in a water solution and swelled to the original column with no structural damage. This result indicates that the crosslinks between the GO sheets were not broken by external compression and that the shrinkage of the aerogels was due solely to the deformation of the GO sheets, which could expand once exposed to an aqueous solution again. This phenomenon is quite consistent with some other 3D aerogels with superior mechanical properties, such as the carbon nanotube-graphene hybrid aerogels,[42] the reduced graphene aerogels after supercritical CO_2 drying,[36] and the biomass-derived sponge-like carbonaceous aerogels.[37,52] Some of them can recover to their original volume completely, and some have very high Young's moduli values in both of the yield region and the elastic region. Of course, the characterization methods through compressive stress-strain curves in these researches provide a good reference for the future study about the structure properties of LDH+GO aerogels.

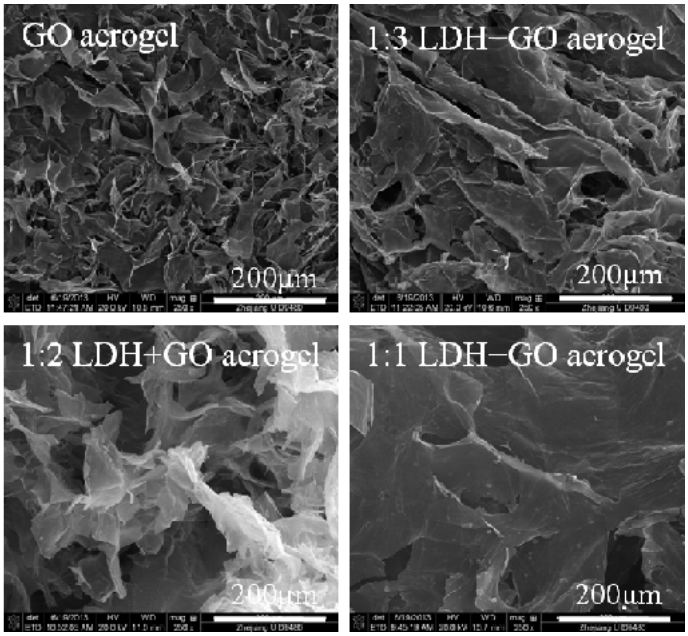

Fig. 2 Scanning electron microscopy (SEM) image of a pure GO aerogel and LDH+GO aerogels with different ratios of LDH and GO.

The scanning electron microscopy (SEM) images in Fig. 2 clearly show a porous 3D GO framework of randomly oriented. The micro-scale morphology of the LDH+GO aerogels largely depended on the added concentration of LDHs. Comparison of the SEM images of the LDH+GO aerogels in Fig. 2 revealed that the greater the added concentration of LDHs, the larger the assembled GO sheets. Obviously, the neat GO aerogels were constructed of numerous assembled GO sheets in a shape of little fractals; when the layered double hydroxides were added, the GO fractal gradually appeared larger in size in proportion to the amount of LDHs added. Especially, The 1:1 LDH+GO aerogel resembled a large piece of flat film in the limited scale of the SEM image. On the basis of these observations, we can assume that the assembly process of LDH+GO hydrogels/aerogels is similar to that of joining pieces of fabric at a tailor's hands in which the GO nanosheets are small rags and the LDHs act as buttons that can interlace the GO nanosheets together and render them into a stable 3D architecture.

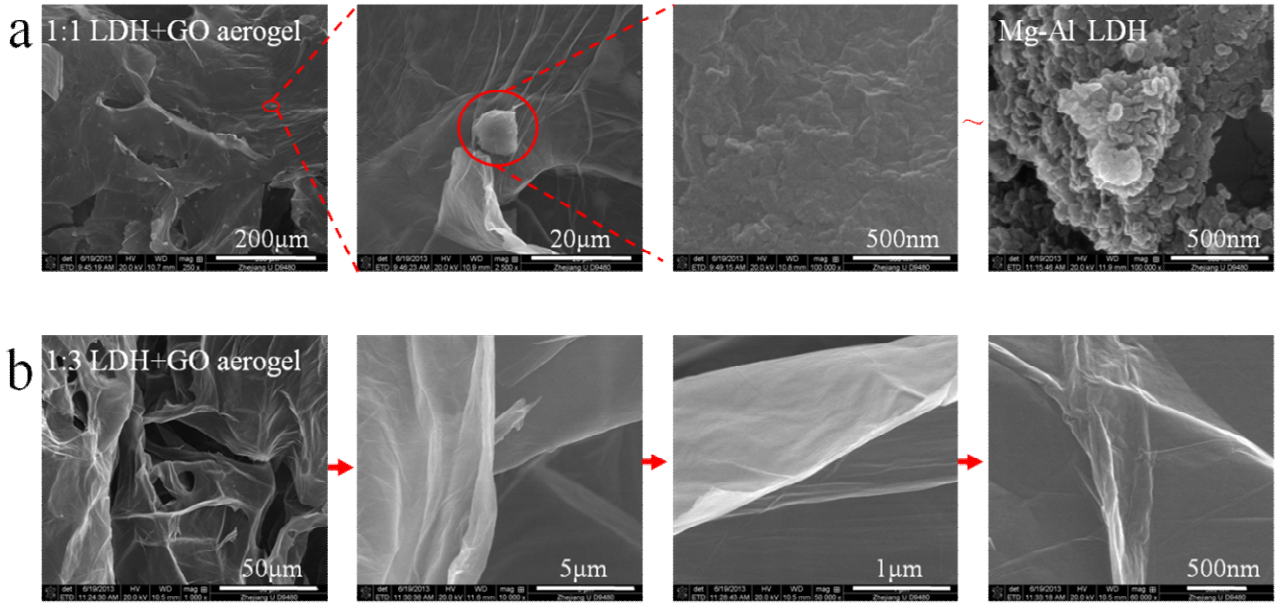

Fig. 3 FE-SEM images of (a) LDHs on the 1:1 LDH+GO aerogel surface and pure LDH powder; (b) a 1:3 LDH+GO aerogel surface, with no observable LDH particles.

Give an insight into the SEM images of different LDH+GO aerogels (Fig. 3), there are solid particles deposited on the surface of the GO sheets remarkably in high LDHs addition aerogel (i.e. 1:1 sample). Increasing the SEM magnification (Fig. 3a) revealed that these particles were residual undispersed LDHs, which possessed the same morphology as pure Mg-Al LDH powders. However, no impurities were observed on the 1:3 LDH+GO aerogel with low LDH (Fig. 3b), even when the SEM magnification was increased to 500 nm; the sheets appeared very glabrous, with folds and crimping. These results indicate that excess LDHs simply agglomerate and are deposited on the surface. However, if the added concentration of LDHs is not in excess, the LDHs will fully function as buttons and disperse to an apparently invisible size in the field emission-scanning electron microscope (FE-SEM) images.

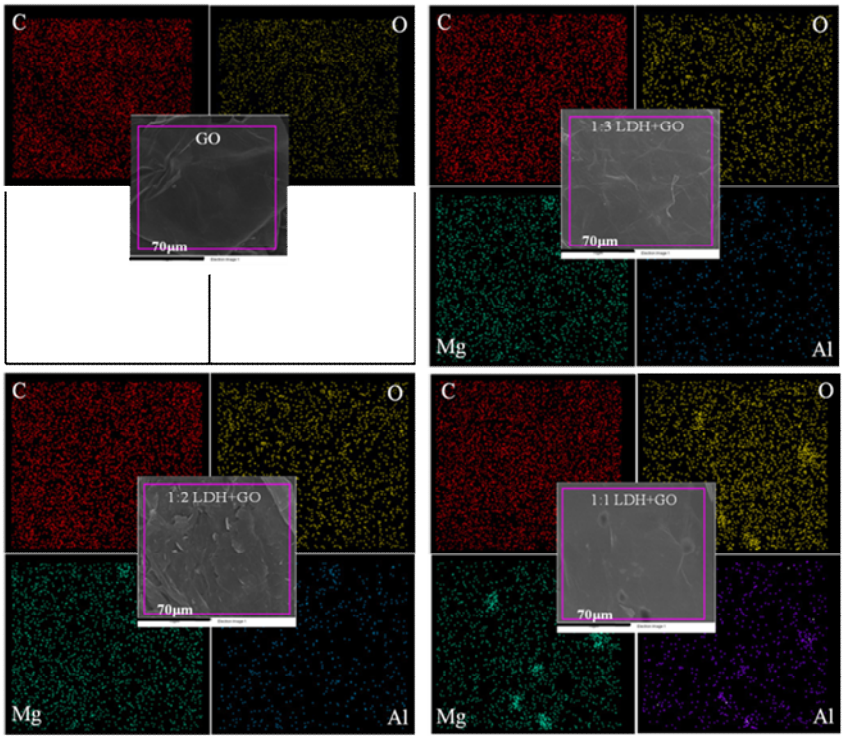

Fig. 4 EDS elemental maps and FE-SEM images (center) of GO and 1:3, 1:2, and 1:1 LDH+GO aerogels.

Energy-dispersive spectrometry (EDS)-elemental mapping images of the corresponding SEM region clearly confirmed the uniform distribution of the metallic elements (Mg and Al) of the LDHs on the GO sheets (Fig. 4). Neat GO aerogels (without added LDHs) only presented the C and O components which come from GO. The metallic elements Mg and Al of the LDHs were scattered evenly in the maps of the 1:3 and 1:2 LDH+GO aerogels. The intensity of the EDS signals increased with the concentration of LDHs. The signals of the C and O elements were stronger than that of the neat GO aerogel, which was ascribed to the interlayer anions of CO_3^{2-} and the hydroxyls of plate from LDHs. Notably, the 1:1 LDH+GO aerogel exhibited a mal-distribution of O, Mg, and Al elements, and the position of the conglomerations in the elemental mapping images corresponded to the dark dots on the SEM images. These results are in agreement with the above discussion that excess LDHs will agglomerate and deposit on GO surface.

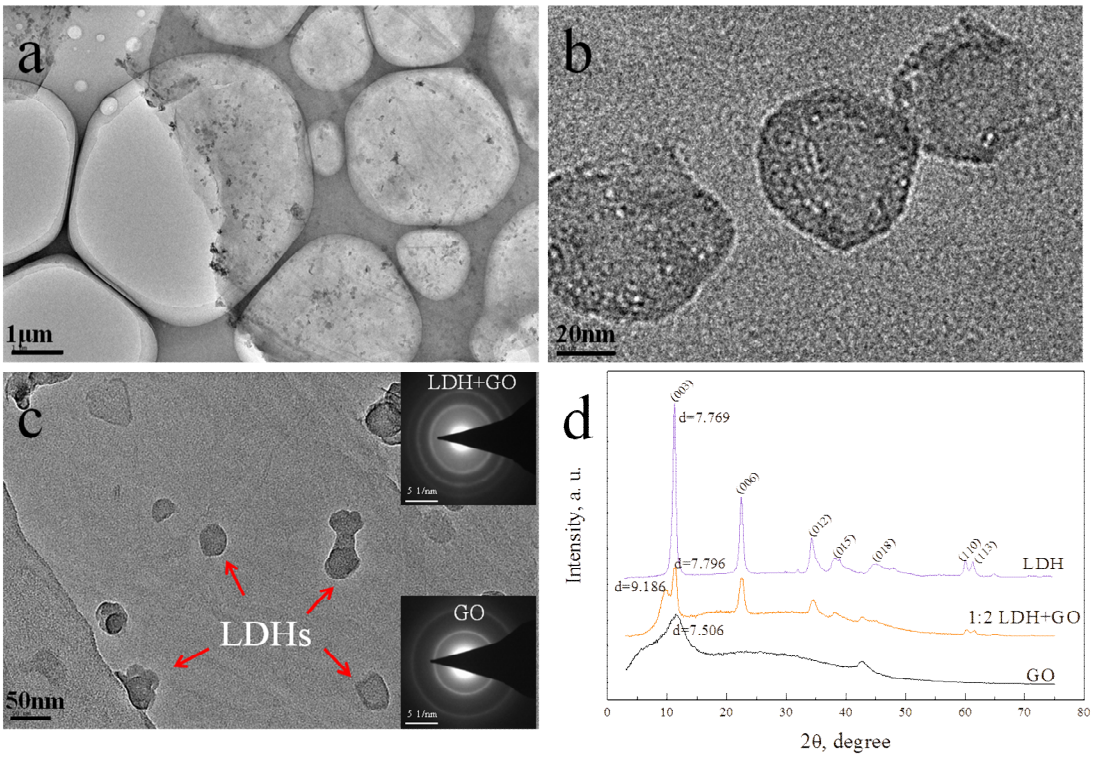

Fig. 5 (a)-(c) HR-TEM images of the 1:2 LDH+GO aerogel with different magnifications, and the corresponding SAED patterns (inset graphs of (c)) of areas with only GO and LDH on GO. (d) XRD patterns of the LDH powder, 1:2 LDH+GO aerogel, and neat GO aerogel.

Selecting a moderate ratio of the 1:2 LDH+GO aerogel as an example, the high-resolution transmission electron microscopy (HR-TEM) images clearly showed nanoscale particles of LDHs distributed in the aerogel with sizes of 20-60 nm (Fig. 5b). Noteworthily, the LDH nanoparticles were encapsulated between several layers of graphene sheets rather than deposited on the external surface of the GO film (presented in Fig. 5a), confirming their function as buttons for splicing the GO nanosheets, which may expose more active adsorption sites. Preliminarily, the selected area electron diffraction (SAED) pattern (the inset graphs of Fig. 5c) of the selected glabrous GO area exhibits two shape diffraction rings, but three shape diffraction rings were observed in the area of the GO containing encapsulated LDHs. The results of polycrystal electron diffraction (which was due to

the overlapping nature of the GO nanosheets) revealed that the extra diffraction ring was due to the crystalline texture of the LDHs and that two different crystal phases undoubtedly co-existed.

XRD analysis (Fig. 5d) was further used to confirm that the plate-like crystal structure of the LDHs was maintained in the LDH+GO aerogels. The pattern of the LDH powder displayed characteristic diffraction peaks of hydrotalcite-like materials (JCPDS No. 89-0461) at 2θ = 11.2^{o} (003), 22.4^{o} (006), 34.4^{o} (012), 38.7^{o} (015), 45.6^{o} (018), 60.0^{o} (110), and 61.2^{o} (113), which can be indexed accordingly.[53,54] Peak fitting (Jada 5.0) indicated that the LDHs in this study are of high crystallinity (88.64%) but with very small crystallites whose sizes were calculated as approximately 130 Å (diameter perpendicular to the crystal plane). All of the corresponding characteristic diffraction peaks of the LDHs were observed in the 1:2 LDH+GO aerogel, and they exhibited similar diffraction peak shapes at 2θ = 30 ~ 40°, which is different from the nanohybrids of graphene (oxide) and LDHs that broad hump peak would appear at this range.[55] This phenomenon suggests that the LDH particles retained their layered crystal structure rather than exfoliating into nanosheets or dissolving into metal ions in the assembly of GO. Furthermore, the interaction of LDHs and GO nanosheets in the LDH+GO aerogels is not a simple disordered stack but the result of self-assembly.[56] Several metal ions have been reported to induce assembly of graphene 3D architectures, including La^{3+}, Fe^{2+}, Ni^{2+}, and Co^{2+},[18,27,28] but it was not the same case in this study. Additional experiments investigating the effect of metallic ion release or exfoliated LDH nanosheets on LDH+GO hydrogel formation have been performed and excluded, which is described in detail in the ESI (Fig. S-1).

The XRD pattern of the neat GO aerogel exhibited a single broad peak at 2θ = 11.78^{o}, corresponding to an interlayer *d* spacing of 7.506 Å. This spacing is mainly attributed to the oxygen-containing group on the GO nanosheets, which leads to interlayer spacing when GO self-assembles into a 3D network via self-physical (or self-chemical) cross-linking after

freeze-drying. However, the width of this peak provides important information: first, neat GO aerogels have small GO sheet sizes (in agreement with the SEM results), and second, the domain order is relatively short or there is a turbostratic arrangement of GO sheets, each of which broadens the diffraction peak.[57] Interestingly, the 1:2 LDH+GO aerogel possessed a double peak located at $2\theta = 9.62^{o}$ and 11.34^{o}, respectively. The higher-intensity sharper peak ($2\theta = 11.34^{o}$) was assigned to the (003) reflection peak from LDHs, while the other peak was assigned to interlayer spacing of the GO sheets, which expanded to 9.186 Å with LDH crosslinking. The peak width was narrower than that of the neat GO aerogel, indicating that the GO sheets were knitted into a larger layer or that a more ordered assembly was present.

A quasi-hexagonal crystal of LDH nanoparticles was observed more directly and clearly on the GO sheet surface using Scanning transmission electron microscopy (STEM) (ESI, Fig. S-2 a), and EDS-elemental mapping gave the two metallic components (Mg and Al) at a scale of 20 nm (Fig. S-2 b and c). As far as here, the metallic composition, uniform distribution, and layered crystal integrity of the LDH nanoparticles were fully confirmed in the LDH+GO aerogels.

The Fourier transform infrared (FT-IR) spectrum (Fig. 6a) of the neat GO aerogel revealed a broad stretching mode of O-H in the region between 3000 cm^{-1} and 3700 cm^{-1}. A shoulder peak at approximately 3600 cm^{-1} was assigned to the free O-H, and the band at 3411 cm^{-1} was assigned to hydrogen-bonded O-H. After LDHs were incorporated into the structure, the free O-H band weakened gradually, and the fixed O-H stretch intensified with the increasing addition of LDHs in the LDH+GO aerogels. This result suggests that more hydrogen bonds were formed between GO and the LDHs because the O-H band for the LDH powder (from interlayer water and M-OH) was also red-shifted from 3498 cm^{-1} to 3411 cm^{-1} upon bonding of LDHs with the GO sheets.[54] It can be notably observed that the C=O vibration from GO at 1729 cm^{-1} disappeared in the LDH+GO aerogels[18], indicating that oxygen-containing functional groups, particularly carbonyl or carboxyl

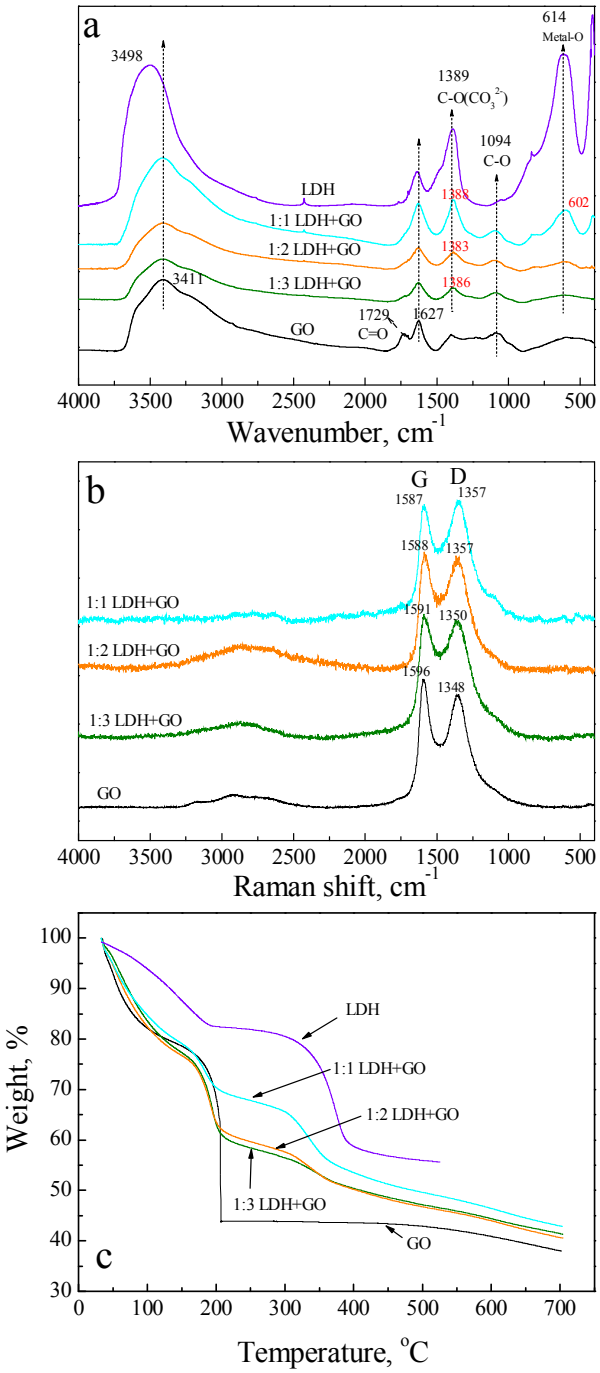

Fig. 6 (a) FT-IR spectra, (b) Raman spectra, and (c) TGA curves of the neat GO aerogel, LDH+GO aerogels with different LDH:GO ratios, and the LDH powder.

groups on GO, participated in bonding with the LDHs. Comparison of the FT-IR spectra of the LDH powder and the LDH+GO aerogels revealed that the band at 1640 cm^{-1}, which originates from a bending vibration of the O-H of LDHs, vanished or is fully covered by a C=C (1627 cm^{-1}) band from GO in the LDH+GO aerogels. In addition, the M-O lattice vibration (M = Mg and Al) shifted from 614 cm^{-1} to 602 cm^{-1} after assembly.[58,59] All of these observations further confirm that the linkages between the GO nanosheets and the LDHs in the LDH+GO hydrogels/aerogels are partially driven by hydrogen bond formation between the external O-H of the LDH plates and the oxygen-containing groups of GO.

As well known, the D band (1348 cm^{-1}) and the G band (1596 cm^{-1}) in Raman spectra are two characteristic peaks for graphene, which correspond to the *K* point phonons of A_{1g} symmetry associated with structural defects and the zone center phonons of E_{2g} symmetry observed for sp^2 carbon domains, respectively.[60,61] Eye-catching from Fig. 6b, a notable blue-shift (1348 cm^{-1}→1357 cm^{-1}) and red-shift (1596 cm^{-1}→1587 cm^{-1}) occurred on the D and G bands, respectively, upon GO assembly into aerogels by LDH cross-linking. These opposing peak shifts indicate that more localized sp^3 defects were brought into the sp^2 carbon network of the GO sheets during the linkage.[40] The intensity ratio of the D to G bands (I_D/I_G) in the LDH+GO aerogels increased from 0.968 for the 1:3 sample to 1.052 for the 1:1 sample, compared to 0.882 for the pure GO aerogel, which further indicates the decreased size of the in-plane sp^2 domains and partially disordered crystal structure of the GO nanosheets.[60,62,63] In brief, the addition of LDHs caused disturbance of the sp^2 carbon network in GO. Of prime importance is the 9-cm^{-1} red-shift of the G band. Similar shifts have been observed previously for GO assembled with epoxy,[19] DNA,[25] and FeOOH,[28] indicating that strong interactions and charge transfer likely account for this Raman observation.[64-66] In addition to improving the electrochemical performance of the LDH+GO aerogels,[31] charge transfer enhances the interaction forces between the LDHs and GO.

Due to the isomorphous substitution of M^{2+} (Mg) by M^{3+} (Al), LDHs possess a positively charged framework, and although their interlayer is balanced by anions, the external surface still behaves positively.[67] Due to the presence of oxygen-containing groups, the electronegativity of GO originates from the ionization of hydroxyl or carboxyl groups,[68] hence electrostatic interaction is an undeniable force. Meanwhile, LDH with positive charge have an analogy to a cation, and the delocalized large π bond on the surface of GO can bind with LDHs via strong lattice-lattice cation-π interactions after charge transfer has occurred. In addition, FT-IR analysis indicated that hydrogen-bonding might be another driving force. LDHs share a proton (H) with the oxygen-containing or the large electron-rich π band of the GO nanosheet surface and form a conventional strong hydrogen bond or an improper weak π hydrogen bond.[69] In an ionic system, the charges strengthen hydrogen bonding by decreasing the donor-acceptor distance and enabling further delocalization of the π system.[69] Therefore, the hydrogen bonds formed between the LDHs and GO sheets will be strengthened because of charge assistance. Of course, van der Waals or other forces might also participate in the interactions between the LDHs and GO sheets. Thus, the high plasticity of the LDH+GO aerogels discussed above can be well understood by taking into the strong interactions between the LDHs and GO nanosheets, which protect the 3D architecture. External compression can incurvate the GO sheet but cannot break the interactions between the LDHs and GO sheets.

Fig. 6c shows the thermogravimetric analysis (TGA) curves in a N_2 atmosphere to analyze the thermal stability of the samples. All of the aerogel samples have a rapid mass loss of approximately 20% before 150 ˚C due to evaporation of the water molecules that were held in the material. However, the mass loss properties of the LDH+GO aerogels in this temperature range are consistent with that of the neat GO aerogel rather than the LDH powder due to the encapsulation of the LDH nanoparticles between several layers of graphene sheets, which protects them from structural water loss. The neat GO

aerogel then displays a significant mass loss (34.69%) from 150 ˚C to 250 ˚C, and this dramatic decrease is ascribed to the decomposition of oxygen-containing groups such as carboxyl and hydroxyl groups. By contrast, although the LDH+GO aerogels display the same onset temperature as the neat GO aerogel, they undergo appreciably less weight loss in the same temperature range of 150 ˚C to 250 ˚C (e.g., 11.28% for the 1:1 sample, 17.06% for the 1:2 sample, and 18.88% for the 1:3 sample). Considering the weak contribution from LDHs for weight loss, the LDH+GO aerogels remain exhibit largely improved thermal stability. For example, addition of the individual weight losses of the LDH powder and neat GO would give 27.45% for the 1:3 LDH+GO aerogel, which is higher than the measured value (18.88%). Therefore, the strong interaction between the LDHs and the GO sheets protects the thermal stability of the LDH+GO aerogels and, in particular, prevents the decomposition of oxygen-containing groups in the GO. The next two steps of mass loss on assembled aerogels are mainly due to the structural degradation of the LDH lattice and the GO carbon substance at high temperature.

Based on the structural analysis and the potential interaction mechanisms, the self-assembly process for GO hydrogels and aerogels by LDH cross-linking is illustrated in Fig. 7.

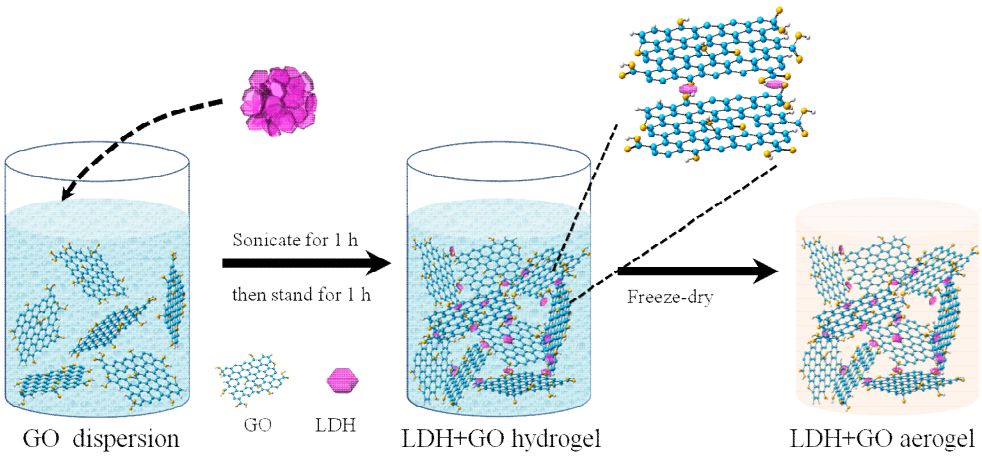

Fig. 7 Schematic synthesis of GO hydrogels and aerogels by LDH cross-linking.

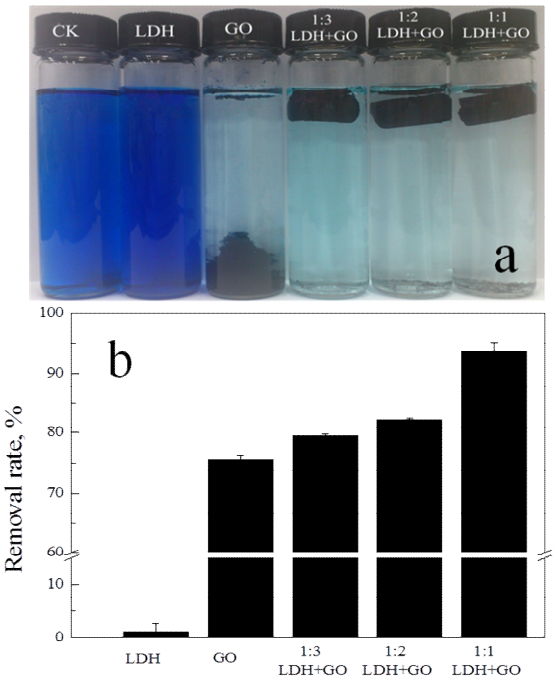

Fig. 8 (a) Photo of methylene blue (MB) solution before and after treatment with the LDH powder, neat GO aerogel, and LDH+GO aerogels with different LDH:GO ratios. (b) Removal rate of MB in the set of (a). The concentration of MB was 20 mg L^{-1}. (40 mL), volume of aerogels: 1 mL.

These assembled LDH+GO aerogels were tested for removal of environmental pollutants. Fig. 8a presented the pre- and post-treatment of 20 mg L^{-1} methylene blue (MB) solution with the synthesized aerogels, and obvious decolorization was observed. The removal rate of MB increased from 79 % of neat GO aerogel to 94% of 1:1 LDH+GO aerogel (Fig. 8b), which acted as high-efficient adsorbents. Their adsorption capacity for MB was 96~125 mg g^{-1}, which is much larger than those with carbon nanotubes as adsorbent (21.8 mg g^{-1}) under similar conditions, and comparable with graphene aerogel and graphene-carbon nanotubes composite aerogel.[42] The contribution from the adsorption on LDH powder can be neglected or excluded, because there was almost no removal of MB calculated in Fig. 8b. The LDH possesses of positively charged frameworks which have shown high performance for anionic pollutants adsorption,[59,70,71] and it has

studied that the nanocomposites of LDHs and GO could high-efficiently remove anionic As (V) below the point of zero charge via electrostatic attraction. MB is one type of cationic dye, so it is reasonable that LDH powders behave no adsorption for MB. However, the role of LDH component in the LDH+GO aerogels in anionic dye removal should be carried out in the future work. It was reported that the MB molecules can be attracted by negatively charged GO sheets and form aggregates on the surface of GO.[72] The contents of GO component in every type of aerogels were same, i.e., 5 mg GO in 1 mL aerogel, as expected that the theoretical adsorption capacities for MB should be same for different LDH+GO aerogels. However, the developed performance of aerogels with the increase of LDH additive amount was observed in Fig. 8b. This was mainly attributed to the LDH in LDH+GO aerogels bond with GO and then knitted the small GO sheet into large one, which reduced the stacking of GO sheet by π-π interaction. Consequently, more active sites can be exposed for binding of large molecule of MB. Compared with neat GO aerogel, another apparent advantage of LDH+GO aerogels is the structural stability in dynamic use and convenience for separation, while neat GO aerogel was fully disintegrated after adsorption in aqueous solution (Fig. 8a).

There have been lots of studies about the applications of graphene oxides for heavy metals adsorption, which were proved to be superior adsorbents.[70,73,74] In fact, GO is a strongly acidic buffer material derived from its rich oxygen-containing groups on surface.[16] However, pH is an important factor affecting heavy metal ions adsorption,[73] especially low pH is unfavourable for their removal because of the competition from H^+. From Fig. 9 about the adsorption of Cd^{2+}, it can be observed that LDH+GO aerogels felicitously solved the acidic buffering effect of GO aerogel (the equilibrium pH (pH_E) changed to 3.9). LDH+GO aerogels maintained the solution pH around neutral closed to blank solution, and kept away from the pH range of Cd^{2+} precipitation at the employed concentration. The inserted graph shows that LDH powder has a negligible adsorption for Cd^{2+}, and the converted amount of sorbed Cd^{2+} (Fig. 9) on the GO component of every aerogel increased from 68.01 mg g^{-1}

of neat GO aerogel to 95.67 mg g^{-1} of 1:1 LDH+GO aerogel, one to two orders of magnitude higher than some conventional adsorbents for Cd^{2+} removal, even compared with their saturated adsorption amount calculated from Langmuir model.[75,76] The improved performance can also be ascribed to that more active sites of GO sheets were exposed under the assistant of LDH nanoparticles. Three models were fitted for the kinetic curves of Cd^{2+} adsorption, and their corresponding regression parameters are listed in Table 1. Both of Pseudo-second-order and Elovich models presented well fitting, and the largest R^2 (0.9418-0.9893) of Elovich model illustrated that the adsorption of Cd^{2+} onto aerogels was a process of diffusion in the 3D architecture or certain heterogeneous reaction occurred in aerogels during Cd^{2+} removal.[77] However, noted that LDH+GO aerogels possessed the significant low rate constants of K_1, K_2 and α than that of neat GO aerogel, and the integral 3D network structure of LDH+GO aerogels should account for it which is different from the barrier-free diffusion in GO aerogel because of monolith disorganization.

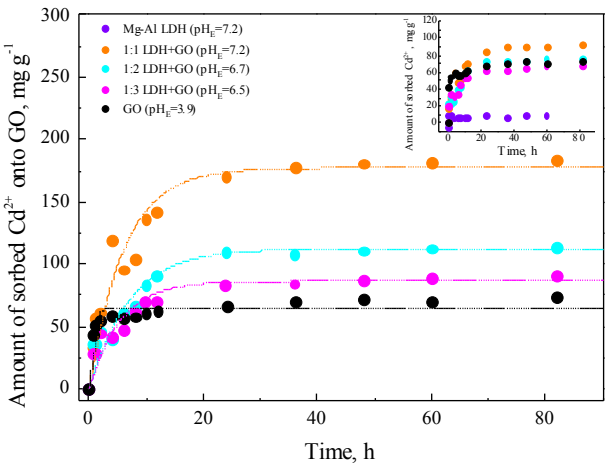

Fig. 9 Time-dependent adsorption of Cd^{2+} on LDH powder, neat GO aerogel, and LDH+GO aerogels with different LDH:GO ratios. The ordinate is the corresponding amount of sorbed Cd^{2+} onto the GO component of LDH+GO aerogels, and the inserted graph is the sorbed amount of Cd^{2+} on different aerogels. Initial concentration of Cd^{2+} was 50 mg L^{-1}, and the equilibrium pH of solution was marked beside the icon.

Table 1 Regression parameters of kinetic models for Cd^{2+} adsorption onto different aerogels at 50 mg L^{-1}.

Samples	Pseudo-first-order model [1)]			Pseudo-second-order model [2)]			Elovich model[3)]		
	q_e (mg g^{-1})	K_1 (h^{-1})	R^2	q_e (mg g^{-1})	K_2 (mg g^{-1} h^{-1})	R^2	β (g mg^{-1})	α (mg g^{-1} h^{-1})	R^2
GO	65.109	1.6012	0.8881	68.012	0.0359	0.9397	0.1806	36961	0.9893
1:3 LDH+GO	64.633	0.1858	0.8984	68.960	0.0045	0.9463	0.0963	105.40	0.9678
1:2 LDH+GO	74.774	0.1432	0.9105	81.211	0.0026	0.9330	0.0795	81.016	0.9418
1:1 LDH+GO	88.594	0.1645	0.9303	95.671	0.0026	0.9623	0.0640	89.262	0.9599

1) The Pseudo-first-order parameters (q_e and K_1) were calculated using the logarithmic form of the equation $q_t = q_e$ (1-e^(-K_1t)), where q_t is the amount sorbed per unit weight of sorbent at t time, mg g^{-1}; t is the time, h; q_e (mg g^{-1}) is the adsorption capacity coefficient at equilibrium time, and K_1 (h^{-1}) is the rate constant. R^2 is regression coefficient.
2) The Pseudo-second-order parameters (q_e and K_2) were calculated using the logarithmic form of the equation $q_t = K_2 q_e^2 t /(1+ K_2 q_e t)$, where q_t is the amount sorbed per unit weight of sorbent at t time, mg g^{-1}; t is the time, h; q_e (mg g^{-1}) is the adsorption capacity coefficient at equilibrium time, and K_2 (mg g^{-1} h^{-1}) is the rate constant. R^2 is regression coefficient.
3) The Elovich parameters (β and α) were calculated using the logarithmic form of the equation $q_t = (1/\beta) \ln(\beta\alpha) + (1/\beta) \ln(t)$, where q_t is the amount sorbed per unit weight of sorbent at t time, mg g^{-1}; t is the time, h; β (g mg^{-1}) is the desorption constant, and α (mg g^{-1} h^{-1}) is the initial adsorption rate. R^2 is regression coefficient.

4. Conclusions

In summary, LDH+GO aerogels have been prepared by a facile self-assembly approach. The LDHs nanoparticles in 3D network acted as cross-linking agent molecules, binding and joining GO nanosheets via multiple interactions. Thus the obtained aerogels exhibit excellent structural stability in aqueous solution, which is superior to the fragile morphology of neat GO aerogels and avoid the utilization restrictions. Besides, the high hydrophilicity of LDH+GO aerogels guarantee the availability of the effective active sites in polar solvents, which is obviously different with the hydrophobic surface of graphene. These advantageous properties make them excellent performance in pollutants control, such as dyes and heavy metals, not only for the large adsorption capacity, but also for their convenient application and collection.

Acknowledgements. This project was supported by the National Basic Research Program of China (2014CB441106), the National Natural Science Foundation of China (Grants 21277120 and 41071210), and the Doctoral Fund of Ministry of Education China (Grant J20130039).

Electronic supplementary information (ESI) Available: The methods for the preparation of GO and Mg-Al LDH, the amounts of GO and LDH used in each sample, the effect of metallic ion release from LDH on hydrogel formation. STEM image of the 1:2 LDH:GO aerogel and corresponding elemental mapping images.

Notes and references

1. G. M. Whitesides and B. Grzybowski, *Science*, 2002, **295**, 2418–2421.
2. J. M. Romo-Herrera, M. Terrones, H. Terrones, S. Dag and V. Meunier, *Nano Lett.*, 2007, **7**, 570–576.
3. S. Nardecchia, D. Carriazo, M. L. Ferrer, M. C. Gutierrez and F. del Monte, *Chem. Soc. Rev.*, 2013, **42**, 794–830.
4. M. J. Allen, V. C. Tung and R. B. Kaner, *Chem. Rev.*, 2010, **110**, 132–145.
5. K. S. Novoselov, V. I. Fal'ko, L. Colombo, P. R. Gellert and M. G. Schwab, K. Kim, *Nature*, 2012, **490**, 192–200.
6. Y. Gao and Z. Tang, *Small*, 2011, **15**, 2133–2146.
7. D. Vanmaekelbergh, *Nano Today*, 2011, **6**, 419–437.
8. D. A. Dikin, S. Stankovich, E. J. Zimney, R. D. Piner, G. H. B. Dommett, G. Evmenenko, S. T. Nguyen and R. S. Ruoff, *Nature*, 2007, **448**, 457–460.
9. Y. Xu, H. Bai, G. Lu, C. Li and G. Shi, *J. Am. Chem. Soc.,* 2008, **130**, 5856–5857.
10. A. J. Patil, J. L. Vickery, T. B. Scott and S. Mann, *Adv. Mater.*, 2009, **21**, 3159–3164.
11. C. N. R. Rao, K. S. Subrahmanyam and A. Govindaraj, *Angew. Chem. Int. Ed.*, 2009, **48**, 7752–7777.
12. W. Cai, R. D. Piner, F. J. Stadermann, S. Park, M. A. Shaibat, Y. Ishii, D. Yang, A. Velamakanni, S. J. An, M. Stoller, J. An, D. Chen and R. S. Ruoff, *Science*, 2008, **321**, 1815–1817.

13. Y. Xu, K. Sheng, C. Li and G. Shi, *ACS Nano*., 2010, **4**, 4324–4330.

14. Z. Xu, Y. Zhang, P. Li and C. Gao, *ACS Nano*., 2012, **6**, 7103–7113.

15. H. Hu, Z. Zhao, W. Wan, Y. Gogotsi and J. Qiu, *Adv. Mater.*, 2013, **25**, 2219–2223.

16. D. R. Dreyer, S. Park, C. W. Bielawski and R. S. Ruoff, *Chem. Soc. Rev*., 2010, **39**, 228–240.

17. E. Morales-Narvaez and A. Merkoci, *Adv. Mater.*, 2012, **24**, 3298–3308.

18. H. Huang, P. Chen, X. Zhang, Y. Lu and W. Zhan, *Small*, 2013, **8**, 1397–1404.

19. S. Ye, J. Feng and P. Wu, *J. Mater. Chem. A*., 2013, **1**, 3495–3502.

20. P. M. Sudeep, T. N. Narayanan, A. Ganesan, M. M. Shaijumon, H. Yang, S. Ozden, P. K. Patra, M. Pasquali, R. Vajtai, S. Ganguli, A. K. Roy, M. R. Anantharaman and P. M. Ajayan, *ACS Nano*, 2013, **7**, 7034–7040.

21. H. Sun, Z. Xu and C. Gao, *Adv. Mater.*, 2013, **25**, 2554–2560.

22. C-H. Zhu, Y. Lu, J. Peng, J-F. Chen and S-H. Yu, *Adv. Mater*., 2012, **22**, 4017–4022.

23. H. Gao, Y. Sun, J. Zhou, R. Xu and H. Duan, *ACS Appl. Mater. Interfaces*, 2013, **5**, 425–432.

24. Q-Y. Cheng, D. Zhou, Y. Gao, Q. Chen, Z. Zhang and B-H. Han, *Langmuir*., 2012, **28**, 3005–3010.

25. Y. Xu, Q. Wu, Y. Sun, H. Bai and G. Shi, *ACS Nano*, 2010, **4**, 7358–7362.

26. C. Huang, H. Bai, C. Li and G. Shi, *Chem. Commun.*, 2011, **47**, 4962–4964.

27. X. Jiang, Y. Ma, J. Li, Q. Fan and W. Huang, *J. Phys. Chem. C*, 2010, **114**, 22462–22465.

28. H-P. Cong, X-C. Ren, P. Wang and S-H. Yu, *ACS Nano*., 2012, **6**, 2693–2703.

29. B. Adhikari, A. Biswas and A. Banerjee, *Langmuir*, 2012, **28**, 1460–1469.

30. J. Li, C. Liu and Y. Liu, *J. Mater. Chem*., 2012, **22**, 8426–8430.

31. W. Chen, S. Li, C. Chen and L. Yan, *Adv. Mater.*, 2011, **23**, 5679–5683.

32. Z. Zhang, F. Xiao, Y. Guo, S. Wang and Y. Liu, *ACS Appl. Mater. Interface*, 2013, **5**, 2227–2233.

33. J. Yuan, J. Zhu, H. Bi, Z. Zhang, S. Chen, S. Liang and X. Wang, *RSC Advances*, 2013, **3**,

4400–4407.

34. Y. Xu, X. Huang, Z. Lin, X. Zhong, Y. Huang and X. Duan, *Nano. Res*., 2013, **6**, 65–76.

35. Y. Xu, Z. Lin, X. Huang, Y. Liu, Y. Huang and X. Duan, *ACS Nano*, 2013, **7**, 4042–4049.

36. X. Zhang, Z. Sui, B. Xu, S. Yue, Y. Luo, W. Zhan, B. Liu, *J. Mater. Chem*. 2011, **21**, 6494–6497.

37. X-L. Wu and A-W. Xu, *J. Mater. Chem. A* 2014, **2**, 4852–4864.

38. F. Meng, X. Zhang, B. Xu, S. Yue, H. Guo, Y. Luo, *J. Mater. Chem*. 2011, **21**, 18537–18539.

39. L. Chen, X. Wang, X. Zhang, H. Zhang, *J. Mater. Chem*. 2012, **22**, 22090–22096.

40. S. Sun and P. Wu, *J. Mater. Chem.*, 2011, **21**, 4095–4097.

41. L. Chen, B. Wei, X. Zhang, C. Li, *Small* 2013, **13**, 2331–2340.

42. Z. Sui, Q. Meng, X. Zhang, R. Ma, B. Cao, *J. Mater. Chem*. 2012, **22**, 8767–8771.

43. Y. Long, C. Zhang, X. Wang, J. Gao, W. Wang and Y. Liu, *J. Mater. Chem.*, 2011, **21**, 13934–13940.

44. H. Bi, X. Xie, K. Yin, Y. Zhou, S. Wan, L. He, F. Xu, F. Banhart, L. Sun and R. S. Ruoff, *Adv. Funct. Mater*., 2012, **22**, 4421–4425.

45. S. Wang, H. Sun, H. M. Ang and M. O. Tade, *Chem. Eng. J.*, 2013, **226**, 336–347.

46. P. J. Sideris, U. G. Nielsen, Z. Gan and C. P. Grey, *Science*, 2008, **321**, 113–117.

47. W. S. Hummers and R. E. Offeman, *J. Am. Chem. Soc.*, 1958, **80**, 1339.

48. Y. Zhao, F. Li, R. Zhang, D. G. Evans and X. Duan, *Chem. Mater*., 2002, **14**, 4286–4291.

49. L. Li, X. L. Liu, H. Y. Geng, B. Hu, G. W. Song, Z. S. Xu, *J. Mater. Chem. A* 2013, **1**, 10292–10299.

50. H. Gao, F. Xiao, C. B. Ching and H. Duan, *ACS Appl. Mater. Interfaces.*, 2012, **4**, 2801–2810

51. Y. Lin, G. Ehlert, C. Bukowsky and H. A. Sodano, *ACS Appl. Mater. Interfaces*, 2011, **3**, 2200–2203.

52. X-L. Wu, T. Wen, H-L. Guo, S. Yang, X. Wang, A-W. Xu, *ACS Nano*, 2013, **7**, 3589-3597.

53. A. Garcia-Gallastegui, D. Iruretagoyena, V. Gouvea, M. Mokhtar, A. M. Asiri, S. N. Basahel, S.

A. Al-Thabiti, A. O. Alyoubi, D. Chadwick and M. S. P. Shaffer, *Chem. Mater.*, 2012, **24**, 4531–4539.

54. F. Millange, R. I. Walton and D. O'Hare, *J. Mater. Chem.*, 2000, **10**, 1713–1720.

55. J. L. Gunjakar, I. Y. Kim, J. M. Lee, N-S. Lee and S-J. Hwang, *Energy Environ. Sci.*, 2013, **6**, 1008–1017.

56. J. L. Gunjakar, T. W. Kim, H. N. Kim, I. Y. Kim and S-J. Hwang, *J. Am. Chem. Soc.*, 2011, **133**, 14998–15007.

57. S. Dubin, S. Gilje, K. Wang, V. C. Tung, K. Cha, A. S. Hall, J. Farrar, R. Varshneya, Y. Yang and R. B. Kaner, *ACS Nano*, 2010, **4**, 3845–3852.

58. L. Zhang, X. Zhang, L. Shen. B. Gao, L. Hao, X. Lu, F. Zhang, B. Ding and C. Yuan, *J. Power Sources.*, 2012, **199**, 395–401.

59. T. Wen, X. Wu, X. Tan, X. Wang and A. Xu, *ACS Appl. Mater. Interfaces*, 2013, **5**, 3304–3311.

60. V. Chandra, J. Park, Y. Chun, J. W. Lee, I-C. Hwang and K. S. Kim, *ACS Nano*, 2010, **4**, 3979–3986.

61. S. Y. Han, I. Y. Kim, K. Y. Jo and S-J. Hwang, *J. Phys. Chem. C*, 2012, **116**, 7269–7279.

62. A. C. Ferrari and J. Robertson, *Phys. Rev. B*, 2000, **61**, 14095–14107.

63. I. Y. Kim, J. M. Lee, T. W. Kim, H. N. Kim, H. Kim, W. Choi and S-J. Hwang, *Small*, 2012, **8**, 1038–1048.

64. B. L. Prasad, H. Sato and T. Enoki, *Phys. Rev. B*, 2001, **64**, 235407.

65. B. Das, R. Voggu, C. S. Rout and C. N. R. Rao, *Chem. Commun.*, 2008, 5155–5157.

66. X. Liu, C. Z. Wang, Y. X. Yao, W. C. Lu, M. Hupalo, M. C. Tringides and K. M. Ho, *Phys. Rev. B.*, 2011, **83**, 235411.

67. A. I. Khan and D. O'Hare, *J. Mater. Chem.*, 2002, **12**, 3191–3198.

68. D. Li, M. B. Muller, S. Gilje, R. B. Kaner and G. G. Wallace, *Nat. Nanotechnol.*, 2008, **3**,

101–105.

69. G. Gilli and P. Gilli, The nature of the hydrogen bond. Outline of a comprehensive hydrogen bond theory. Oxford University Press. New York. 2009.

70. X-L. Wu, L. Wang, C-L. Chen, A-W. Xu and X-K. Wang, *J. Mater. Chem.*, 2011, **21**, 17353–17359.

71. Y. Lin, Q. Fang, B. Chen, *Chem. Eng. J.* 2014, **237**, 38–46.

72. Y. Chen, L. Chen, H. Bai and L. Li, *J. Mater. Chem. A*, 2013, **1**, 1992–2001.

73. G. Zhao, J. Li, X. Ren, C. Chen and X. Wang, *Environ. Sci. Technol.*, 2011, **45**, 10454–10462.

74. H-L. Ma, Y. Zhang, Q-H. Hu, D. Yan, Z-Z. Yu and M. Zhai, *J. Mater. Chem.*, 2012, **22**, 5914–5916.

75. V. C. Srivastava, I. D. Mall, I. M. Mishra, *Chem. Eng. Process*. 2009, **48**, 370–379.

76. H. Yanagisawa, Y. Matsumoto, M. Machida, *Appl. Surf. Sci*. 2010, **256**, 1619–1623.

77. J. Zhang and R. Stanforth, *Langmuir*, 2005, **21**, 2895–2901.